RESEARCH PAPER

Magnetized Nanocomposite of Sea Shell and Walnut Shell-waste as Adsorbent for Efficient Removal of Methylene Blue

Maryam Bordbar *, Neda Negahdar, and Bahar Khodadadi

Department of Chemistry, Faculty of Science, University of Qom, Qom 37185-359, Iran

ARTICLE INFO

ABSTRACT

In this paper, nano magnetized composite of sea shell (SS) and walnut shell-waste based activated carbon (WAC), (SS/WAC/Fe_3O_4), was synthesized and used for the removal of methylene blue (MB) from an aqueous solution. Field emission scanning electron microscopy (FESEM), energy dispersive X-ray spectroscopy (EDS), Fourier-Transform infrared (FT-IR) spectroscopy, X-ray diffraction analysis (XRD) and UV-Vis were used to characterize the SS/WAC/Fe_3O_4 nanocomposite. The SS/WAC/Fe_3O_4 nanocomposite proved to be an effective adsorbent in the adsorption of methylene blue (MB) in the optimized effective parameters. Effective parameters such as pH, adsorption time (min), adsorbent dosage (g/L) and initial dye concentration were optimized with Box-Behnken Design (BBD). Optimal adsorption conditions including pH=6.5, dye concentration of 4.0 mg L^{-1}, adsorbent amount of 0.232 g L^{-1} and contact time of 40 min were obtained. Fitting the experimental equilibrium data to various isotherm models such as Langmuir and Freundlich models show the suitability and applicability of the Langmuir model. The maximum monolayer sorption capacity was 37.2 mg g^{-1}. More than 93% removal efficiency for MB dye showed that this adsorbent is an effective natural compound and also inexpensive for treatment processes. Therefore, using this method and process to remove dye pollutants from aqueous media is recommended.

INTRODUCTION

Daily release of large amounts of dyes through wastewater from various industries such as textiles, leather, paper and plastics can be very dangerous to the environment. Due to their complex structure, dyes are often stable and resistant to biodegradation, which are often toxic, carcinogenic and mutagenic [1, 2]. Production of toxic amines through reduction and breaking of azo bonds is another problem of depletion of dyes into water sources, which leads to severe effects on vital human organs such as the brain, liver, kidneys, reproductive system and central nervous system [3]. Very small amounts of dyes are clearly visible in the water and may be toxic to organisms in the water. Therefore, the removal of dyes from the process or wastewater will have an impact on the environment.

The methods used to remove dyes mainly include physical, chemical and biological methods [4]. Most of these methods are costly and lead to the production of sludge and even dangerous by-products. Among these methods, the adsorption process by inexpensive adsorbents including clay,

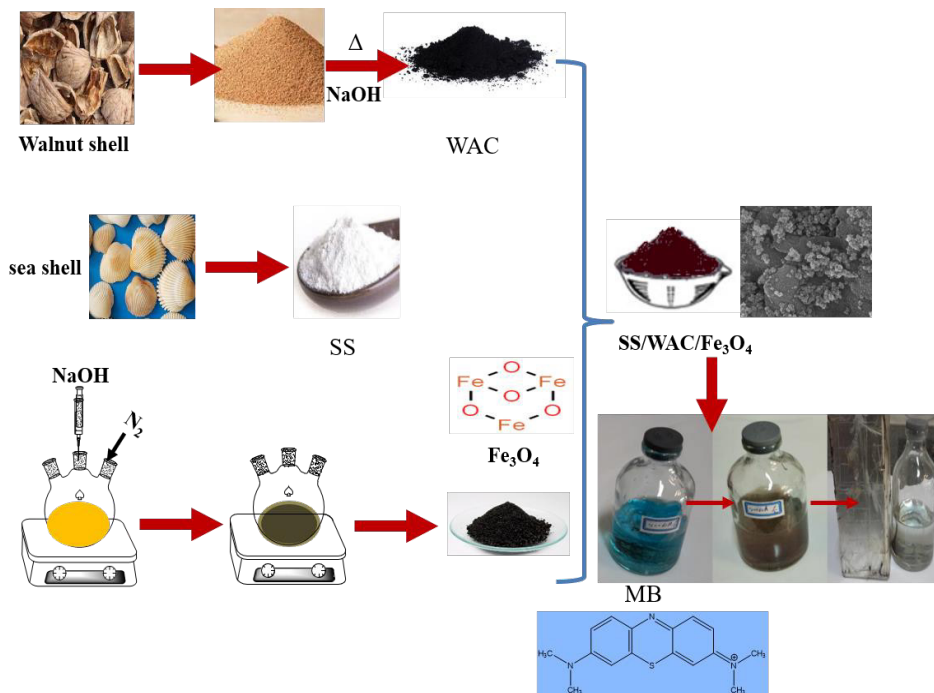** Corresponding Author Email: m.bordbare@gmail.com*

Fig. 1. Schematic illustration of SS/WAC/Fe$_3$O$_4$ nanocomposite preparation and MB removal by it.

zeolites, silicates, agricultural wastes, bio-sorbents in terms of initial cost, wastewater reuse, simplicity and flexibility in design, easy operation and non-toxicity is a superior method. Production of high-quality effluent and no formation of hazardous substances such as ozone and free radicals are other advantages of this method [5].

Many studies have been conducted to find suitable adsorbents to reduce the concentration of colorants in water, including activated carbon [6, 7], peat [8, 9], chitin [10-12], silica [13], and others [14-16].

In recent years, many adsorbents based on agricultural wastes (also activated carbon and by-products such as almond shell [5], glossogyne tenuifolia leaves [17], lignocellulosic waste [18] have been reported and applied for the removal of ionic and nonionic dye molecules from water.

Activated carbon (AC) is considered as a non-toxic adsorbent and universal adsorbent for the removal of pollutants such as dyes and heavy metals from the wastewater due to its high surface area, porous structure, high adsorption capacity, fast adsorption kinetics and general material as support for loading nanomaterials. AC contain various reactive sites such OH, COOH and C=O groups which together with the nanoparticle properties synergically improve the efficiency of adsorption procedure [19].

Unfortunately, two important disadvantages of using activated carbon as an adsorbent include: 1) activated carbon is difficult to separate from the solution and, after use in water and wastewater treatment, is discarded with process sludge, leading to secondary contamination [20]. 2) The cost of AC is relatively high and they are difficult to reproduce, which limits the use of activated carbon in paint wastewater treatment.

To overcome these problems, many researchers and scientists are developing magnetic adsorbents from low-cost materials available as alternatives to activated carbon materials. But these alternative materials must have sufficient adsorption capacity as well as good reproductive capacity.

On the other hand, because of their ease of control and rapid separation, magnetized sorbent have recently been used in water treatment [21, 22] and used to remove dyes and other water molecules [23-25]. The higher adsorption capacity of magnetic adsorbents for cationic basic dyes has been attributed to the interactions of hydroxyl groups with dye molecules [26].

It is also important to combine a low-cost material (such as seashell) with activated carbon that reduces its consumption in the production of composite adsorbents.

The main objective of this work is to introduce new magnetic adsorbent from sea shell (SS) and activated carbon (WAC) that produced from walnut (SS/WAC/Fe$_3$O$_4$ nanocomposite) and study the adsorption potential of SS/WAC/Fe$_3$O$_4$ nanocomposite for the removal of methylene blue (MB) dye from aqueous solution) Fig. 1). The effects of several operating parameters such as pH of solution, adsorbent dosage, initial MB dye concentration and adsorption time on the MB dye adsorption were investigated and optimized by Box-Behnken design (BBD) combined with response surface methodology (RSM).

The adsorption mechanism of MB dye onto SS/WAC/Fe$_3$O$_4$ nanocomposite is also investigated in this report. However, there is no information available in literature regarding the optimization of MB dye adsorption on SS/WAC/Fe$_3$O$_4$ nanocomposites.

MATERIALS AND METHODS

Instruments and reagents

Iron(III) chloride hexahydrate (FeCl$_3$.6H$_2$O), Iron(II) chloride tetrahydrate (FeCl$_2$.4H$_2$O) Nitric acid, Hydrochloric acid, sodium hydroxide and Methylene blue with the highest purity available were purchased from Merck chemical company. By dissolve 100 mg of solid dye in 500 ml of double-distilled water was prepared the MB stock solution (200 mg L1), and dilute it appropriately to obtain the daily working concentration. The high-purity chemicals come from the chemical companies Merck and Aldrich. A Varian model 640 spectrophotometer was used to record FT-IR spectra using pressed KBr pellets. A double beam Perkin-Elmer Lambda 25 spectrophotometer was used to record UV-Vis spectra to ensure the formation of nanoparticles. A Philips model X'PertPro diffractometer (Cu Ka = 1.5406 Å) was used to carry out X-ray diffraction (XRD) measurements at a scanning rate of 2º/min in the 2θ range (10-80). Scanning electron microscopy (SEM) was performed on a TESCAN model VEGA3-XMU equipped with energy dispersive spectroscopy (EDS) analysis. FESEM images were recorded using TESCAN MIRA3 FESEM operating at 15 kV. The chemical compositions of the prepared nanostructures were determined by EDS (energy dispersive X-ray spectroscopy) performed in FESEM. The BET specific surface area (S$_{BET}$), pore volume (micropore volume, V$_{mi}$; and total pore volume, V$_T$), and pore size distribution of the prepared magnetic adsorbent were determined by N$_2$-physisorption using the surface area analyzer model Autosorb-1C (Quantachrome, USA). The multipoint Brunauer, Emmett, and Teller (BET) surface area was determined from the nitrogen adsorption/desorption isotherm. The BET isotherm equation is typically applied on the adsorption isotherm in P/P$_0$ range of 0.02-0.99. Prior to the measurement, the sample was degassed at 200 °C for 6 h in an out-gassing station to remove any adsorbed water or entrapped gases in the sample.

Synthesis of Fe$_3$O$_4$ nanoparticles

The magnetization of alternative ferrite nanoparticles synthesized by co-precipitation method depends more on parameters such as reaction temperature, suspension pH, initial molar concentration , etc. [27].

In a typical synthesis, FeCl$_3$. 6H$_2$O (1.1 g) and FeCl$_2$.4H$_2$O (0.54 g) were dissolved in 100 ml of distilled water under constant stirring and blowing nitrogen for 60 min. The resulting solution is then placed in an oil bath adjusted at 85 °C. Afterwards, NaOH (25 mL and 5 M) as the pH controller agent was subsequently added dropwise to the solution under stirring and blowing nitrogen to reach pH value 10. After that, the solution is then kept in an oil bath at 85 °C under a nitrogen atmosphere for 30 minutes. Finally, the brown precipitates were washed several times with ethanol and distilled water and dried at 60 °C for 24 h.

Preparation of activated carbons from walnut shell (WAC)

In the usual synthesis, the waste walnut shells are first washed with distilled water and dried at 90°C for 6 hours in an oven, and mechanically pretreated by crushing in a mill, therefore, 5 g of walnut shell was washed several times with distilled water. Afterwards, the walnut shell was heated at 450 °C for 20 min. The resulting product was then mixed with NaOH (3:1, NaOH: walnut shell) and heated at 400 °C for 25 min. After that, the black product was washed several times with distilled water. Finally, the final product obtained was dried at 120 °C for 4 h [28].

Preparation of magnetized sea shell and Walnut shell based activated carbon (SS/WAC/Fe$_3$O$_4$)

The synthesis method was referring to some reported work [27, 29]. In brief, as-prepared Fe$_3$O$_4$

Table 1. Independence factors and corresponding levels for optimization.

Variables	Real Values of coded levels		
	-1	0	+1
X_1: pH	3	6.5	10
X_2: adsorbent dosage (g L^{-1})	0.048	0.176	0.3
X_3: initial MB dye concentration (mgL^{-1})	1	5.5	10
X_4: adsorption time (min)	10	35	60

Table 2. Box-Behnken design matrix and related experimental and predicted responses.

Runs	pH	adsorbent dosage	MB dye concentration	adsorption time	$Y_{Experimental}$	$Y_{Predicted}$
		(g L^{-1})	(mgL^{-1})	(min)		
1	3.0	0.048	5.5	35	61.699	57.215
2	6.5	0.300	5.5	60	97.818	97.263
3	10.0	0.176	10.0	35	72.603	71.106
4	6.5	0.048	5.5	60	58.535	61.844
5	6.5	0.176	1.0	60	94.825	94.199
6	10.0	0.176	5.5	60	85.102	82.490
7	3.0	0.176	10.0	35	62.3819	65.895
8	6.5	0.176	5.5	35	90.002	89.999
9	10.0	0.048	5.5	35	59.194	59.369
10	6.5	0.048	5.5	10	41.012	45.185
11	6.5	0.300	5.5	10	82.249	82.598
12	6.5	0.176	5.5	35	90.489	89.999
13	6.5	0.176	5.5	35	89.507	89.999
14	10.0	0.300	5.5	35	98.069	97.598
15	10.0	0.176	1.0	35	94.0374	94.168
16	6.5	0.176	1.0	10	88.001	81.801
17	3.0	0.176	5.5	10	58.950	62.847
18	6.5	0.176	10.0	10	58.680	54.276
19	6.5	0.300	1.0	35	94.183	98.263
20	3.0	0.176	5.5	60	90.589	87.803
21	6.5	0.300	10.0	35	86.352	88.229
22	6.5	0.048	1.0	35	76.845	76.319
23	3.0	0.300	5.5	35	97.097	91.817
24	10.0	0.176	5.5	10	71.980	76.153
25	6.5	0.048	10.0	35	40.123	37.341
26	3.0	0.176	1.0	35	86.244	91.386
27	6.5	0.176	10.0	60	70.100	73.17

(200 mg) nanoparticles were dispersed in a 0.1 mol L^{-1} HNO_3 solution for 10 min, then followed by washing with deionized water several times. Subsequently, the treated magnetic nanoparticles were dispersed in 25 mL solution contain 0.1 g seashell and 0.1 g activated carbon that obtained from walnut shell, under vigorous stirring for 20 min. After stirring for another 20 min in ultrasonic bath, the solution was transferred to a Teflon-sealed autoclave and kept at 180 °C for 12 h then cooled naturally. The resulting product was separated with a magnet and washed several times with deionized water and ethanol was dried at 60 °C for 12 h.

In order to achieve the role of seashell as well as activated carbon in adsorption efficiency, in addition to $SS/WAC/Fe_3O_4$ magnetic nanocomposites, WAC/Fe_3O_4 and SS/Fe_3O4 samples were also prepared as mentioned above.

Experimental design

Box-Behnken experimental design (BBD) was used to investigate the adsorption efficiency (or MB removal percentage) of $SS/C/Fe_3O_4$ for MB (response). Minitab software (version 14) was used to design of experiments and analysis of the experimental results. As shown in Table 1, a three-level BBD was employed to evaluate the significance of the effects of parameters including pH of solution, adsorbent dosage (g L^{-1}), initial MB dye concentration (mgL^{-1}) and adsorption time (min) and a total of 27 runs were carried out (Table 2). The order of the experiments was randomized to minimize the effects of uncontrolled factors.

A second-order polynomial equation was utilized to fit the MB removal percentage as presented in the following Eq:

$$Y_{Predicted} = \beta_0 + \sum \beta_i x_i + \sum \beta_{ii} x_i^2 + \sum \beta_{ij} x_i x_j + \varepsilon \qquad (1)$$

Where $Y_{predicted}$ is the predicted response MB removal percentage. The parameter β_0 is the constant coefficient and β_i is the linear coefficient of the input parameter, β_{ii}, are the quadratic coefficients, β_{ij}, are the different interaction coefficients between input parameters, while X_i and X_j represent the independent variables and ε is the error of the model [30, 31].

Adsorption isotherms

The adsorption experiment was carried out in a batch mode as follows: 0.232 g L^{-1} dosage of SS/WAC/Fe_3O_4 adsorbent, initial concentration of dye was 1–10 ppm and the pH of the solution was retained 6.5 using 0.1 M NaOH and 0.1 M HCl solution. The different concentration solutions were positioned in the water bath shaker at 100 rpm for 40 min. The aliquots for MB were examined in UV–Vis Spectrometer at the wavelength of 667 nm.

Measurements of dye uptake

The dye concentrations were determined according to calibration curve obtained at maximum wavelength (667 nm) over working concentration range. The efficiency of MB removal was determined at different experimental conditions optimized according to the BBD method. The experiments were also performed in the initial MB concentration range of 1-10 mg L^{-1} to obtain adsorption isotherms. The percentage of MB removal is calculated using the following formula:

$$\% \text{ MB removal} = ((C_0 - C_t)/C_0) \times 100 \qquad (2)$$

Where C_0 (mg L^{-1}) and C_t (mg L^{-1}) are the target concentrations at the beginning and subsequent time t respectively. The adsorbed MB amount (q_e (mg g1)) was calculated by the following mass balance relationship:

$$Qe = (C_0 - C_e)V/W \qquad (3)$$

Where C0 and Ce (mg / L) are the initial concentration and equilibrium concentration of the dye in the aqueous solution, V

where C_0 and C_e (mg L^{-1}) are the initial concentration and equilibrium concentration of the dye in the aqueous solution, respectively. Also, V (L) and W (g) are the volume of the solution and the mass of the adsorbent, respectively.

RESULTS AND DISCUSSION
Characterization of SS/WACC/Fe_3O_4

The FT-IR spectra of Seashell, activated carbon, Fe_3O_4 and SS/WAC/ Fe3O4 are shown in Fig. 2. The strong band at 1014 cm^{-1} in the FTIR of WAC spectrum can be attributed to C-C coupling. 400 to 600 cm^{-1} refers to the metal-oxygen (Fe-O) stretching mode in the Fe_3O_4 structure [32]. The FT-IR spectrum data obtained for seashell shows the absorption bands of at ~1463 cm^{-1}, ~1083 cm^{-1}, ~858 cm^{-1}, and ~714 cm^{-1}, which are described
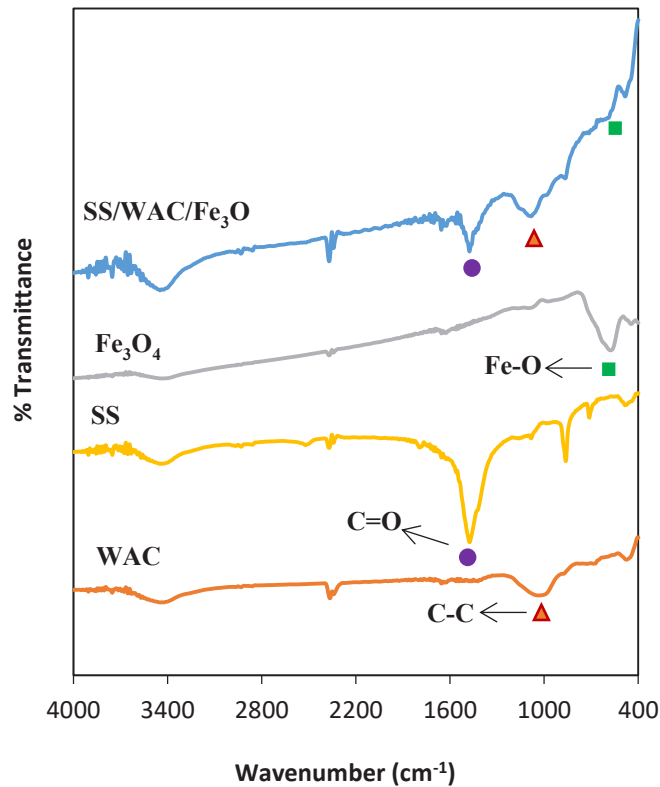
Fig. 2. FT-IR spectra of SS, WAC, Fe_3O_4 and SS/WAC/Fe_3O_4 nanocomposite.

as characteristics of carbonate ions in calcium carbonate and it is the main vibration mode of this particular compound [33]. The band at 3450 cm^{-1} is attributed to (O-H) vibrations in hydroxyl groups. The band appearing at 1770.71 cm^{-1} is attributed to carbonyl (C=O) groups. The appearance of band at 1143 cm^{-1} can be assigned to (C-O) stretching vibrations. The peak at around 889.21 and 669.32 cm^{-1} is ascribed to the aromatic C-H out of-plane vibrations [34]. The FT-IR analysis of SS/WAC/Fe_3O_4 confirm that there was no change in functional groups.
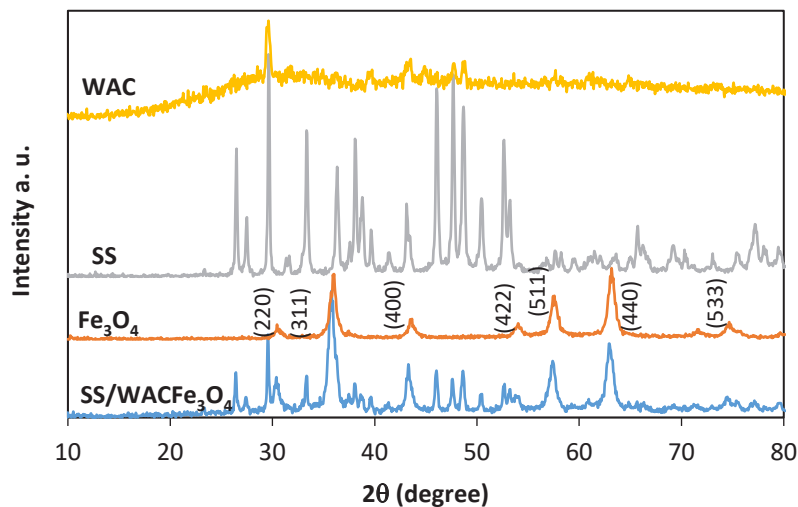

Fig. 3. XRD patterns of SS, WAC, Fe_3O_4 and SS/WAC/Fe_3O_4 nanocomposite.

Fig. 3 shows the X-ray diffraction patterns of shells, activated carbon, Fe_3O_4 and SS/WAC/Fe_3O_4 nanocomposites. Analysis of the diffraction pattern of Fe_3O_4 shows a cubic spinel structure and corresponding to the ICDD card no 01-1111, which is characteristic of this phase due to the strong reflection on the (311) plane. The peaks designated as (220), (311), (400), (422), (511), and (440) planes correspond to the characteristics of the cubic unit cell of the cubic spinel structure [35]. After calculating the grain size with the Scherer formula, we get the Fe_3O_4 particle size as 20.22 nm.

In the XRD pattern of seashell (SS) corresponding to the ICDD card no 05-0453, the peak at $2\theta = 29.5$ is the characteristic peak of aragonite ($CaCO_3$) [36]. The XRD diffraction pattern of Fe_3O_4, SS and WAC is compared with the XRD pattern of SS/WAC/Fe_3O_4 in Fig. 3, which only confirms the presence of SS, WAC and Fe_3O_4 compounds in SS/WAC/Fe_3O_4.

Field emission scanning electron microscopy (FE-SEM) is used to observe the surface physical surface morphology of Seashell, Fe_3O_4 and SS/WAC/Fe_3O_4 (Fig. 4). Fe_3O_4 has a spherical structure with a size in the range 40-60 nm, and walnut activated carbon (WCA) has a microporous structure. SEM image of the WAC is shown in Fig. 4. Many pores are clearly visible on the surface of the WAC. The morphology of seashell indicates that the seashell has a sheet like structure. FE-SEM of the SS/WAC/Fe_3O_4, clearly shows the presence of SS, WAC and Fe_3O_4 is clearly visible.

The elemental composition of the SS/WAC/Fe_3O_4 nanocomposite was also analyzed by EDS spectroscopy (Fig. 5), which also showed C (12.73%), Ca (22.73%), O (54, 33%) and Fe (10.65 %) in the SS/WAC/Fe_3O_4 nanocomposite; in addition, the elemental mapping image confirmed the presence of C, Ca and Fe (Fig. 6).

The hysteresis curve of the SS/WAC/Fe_3O_4 nanocomposite measured at a magnetic field of 8 to +8 kOe and room temperature (298 K), is shown in Fig. 7, showing superparamagnetic properties and high saturation magnetization. From 0 to 8 kOe, the magnetization (M) increases sharply; M is almost saturated at around 2
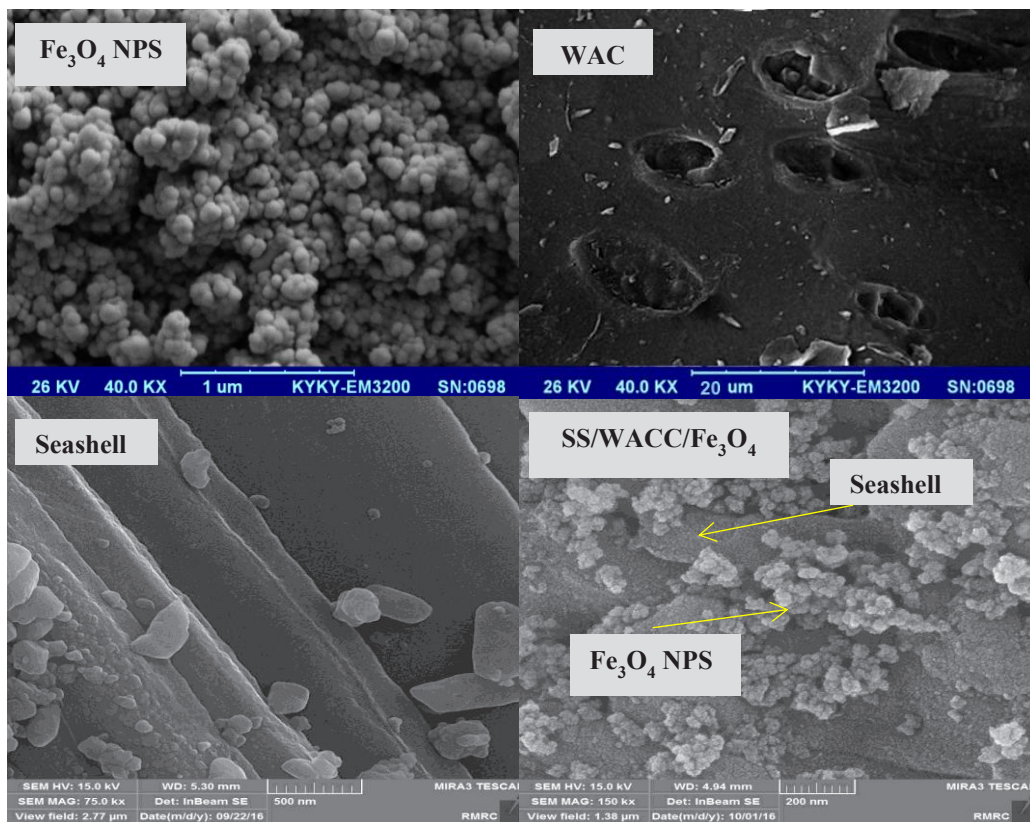

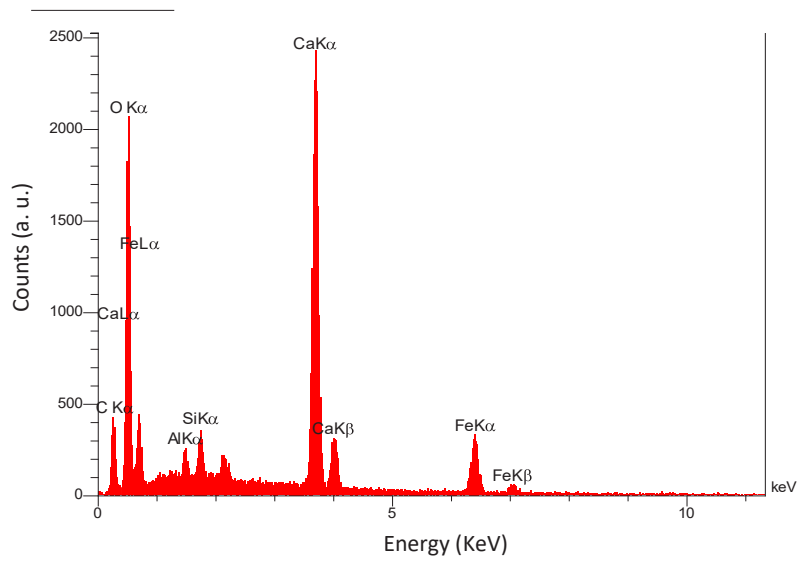Fig. 4. SEM and FE-SEM of the SS, WAC, Fe3O4 and SS/WAC/Fe_3O_4 nanocomposite.

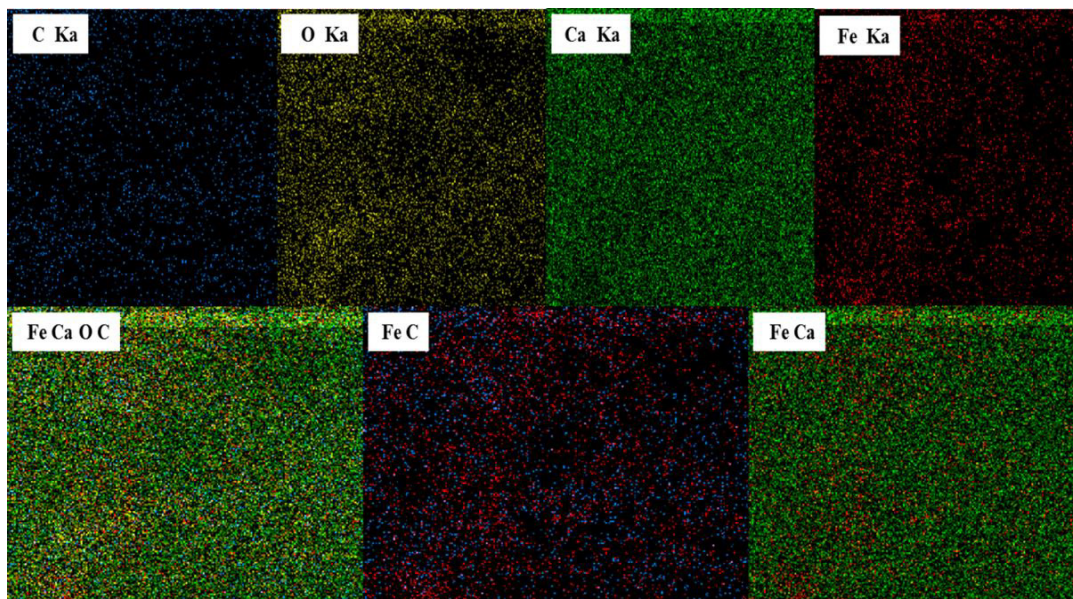Fig. 5. EDS spectrum of SS/WAC/Fe$_3$O$_4$ nanocomposite.

Fig. 6. EDS elemental mapping of the SS/WAC/Fe$_3$O$_4$ nanocomposite

kOe. For SS/WAC/ Fe$_3$O$_4$ nanocomposites, the saturation magnetization (M$_s$) is about 23.97 emu/g, and the reported specified M$_s$ value is 84 emug1 for bulk Fe$_3$O$_4$ particles and 65 emug1 for Fe$_3$O$_4$ nanoparticles [37, 38]. The measured magnetization of nanocomposite was found to be considerably lower than the values measured from bulk magnetite [39].The decrease in saturation magnetization of SS/WAC/Fe$_3$O$_4$ nanocomposite

can be attributed to the decrease in Fe$_3$O$_4$ content in the composite and the diamagnetic contribution from SS and WAC, but it was still large enough to be used as magnetically separable adsorbent.

The determination of the iodine value is usually an additional test of the N$_2$/77 K adsorption isotherm, which is used to measure the surface of the microspores in the pores of the material. The specific surface area (SSA) is a measure of
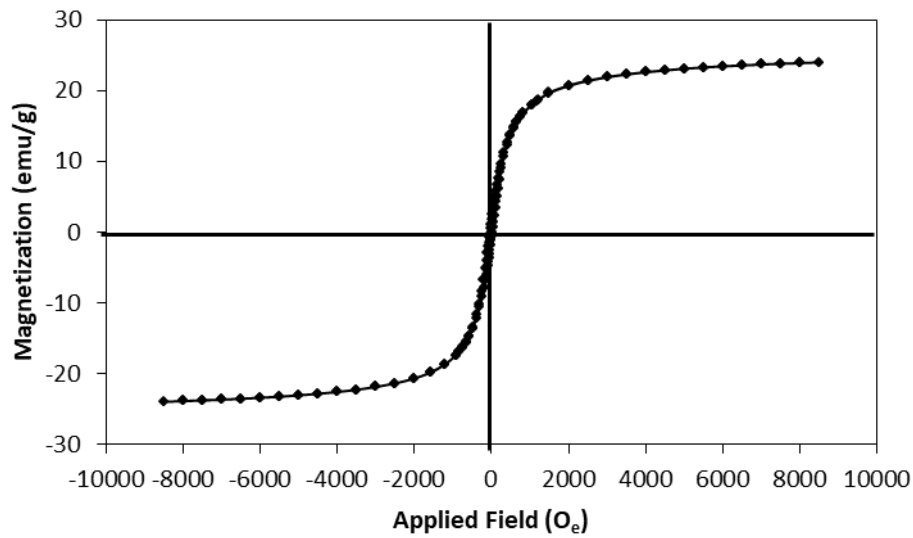
Fig. 7. Vibrating sample magnetometer curve of SS/WAC/Fe$_3$O$_4$ nanocomposite at room temperature

the adsorbent surface area per unit mass and generally depends on the surrounding phase that can modify the surface [40].

The pore size distribution, surface area and N$_2$ adsorption/desorption isotherm of SS/WAC/Fe$_3$O$_4$ nanocomposite are analyzed by BET analyzer as shown in Fig. 8. The surface area of the SS/WAC/Fe$_3$O$_4$ nanocomposite is found to be 101.75 m^2 g$^-$1 which is slightly greater than the surface area of a-Fe$_2$O$_3$ (14.6 m^2 g^{-1}), Fe$_3$O$_4$-C spindles (35.1 m^2 g^{-1}) [41] and limestone (12 m^2 g^{-1}) [42] as reported in the literature. The BJH pore size distribution is used to determine the pore volume of SS/WAC/Fe$_3$O$_4$ nanocomposite. The total pore volume and average pore diameter are 0.2358 cm^3/g and 1.29 nm, respectively. The loop of the adsorption/

desorption curve indicates type-IV adsorption isotherm. The particles are highly mesoporous and have uniform pore size [40].

Determine the isoelectric point of SS/WAC/Fe$_3$O$_4$ nanocomposite

Prepare 0.1 M NaCl solutions with initial pH (pH$_i$) adjusted from 2 to 10 with HCl and NaOH. Take 10 flasks with a capacity of 50 mL for each 0.05 g SS/WAC/Fe$_3$O$_4$ bottle, add 25 mL NaCl solution was prepared above, for 24 h, then filter the solution and redefine the pH (pH$_f$) of the solutions. The results from Fig. 9 determine the isoelectric point of SS/WAC/Fe$_3$O$_4$ is equal to 7.2. This shows that when pH < pH$_{pzc}$, the surface of SS/WAC/Fe$_3$O$_4$ nanocomposite is positively charged,
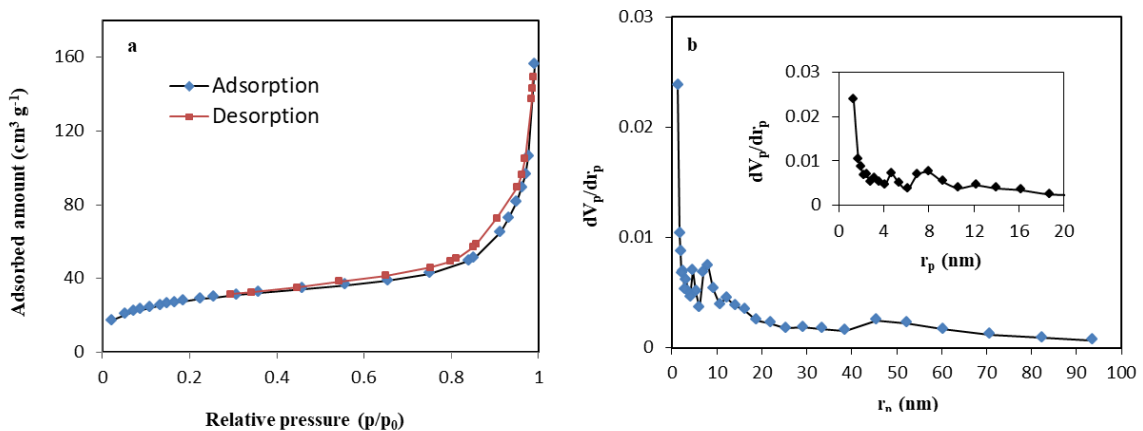

Fig. 8. BET adsorption-desorption isotherm (a) and pore size distribution curves (b) of SS/WAC/Fe$_3$O$_4$ nanocomposite
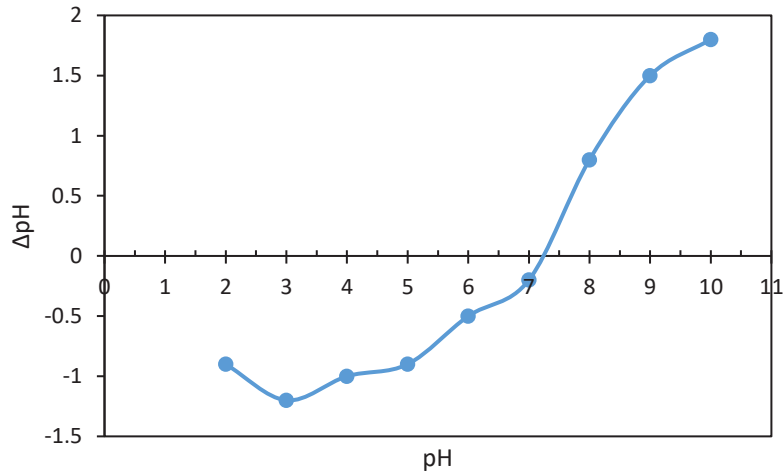
Fig. 9. The graph for determine the isoelectric point of SS/WAC/Fe$_3$O$_4$ nanocomposite

when pH > pH$_{pzc}$, the surface of SS/WAC/Fe$_3$O$_4$ nanocomposite is negatively charged.

Optimization of MB removal parameters by SS/WAC/Fe$_3$O$_4$ nanocomposite

In the BBD step, the adsorption experiments were carried out according to the design matrix (Table 3) and the main, interaction and quadratic effects were evaluated. Four independent variables at three levels were selected, and the responses of 27 experiments were reconstructed and presented in Table 3. Analysis of variance (ANOVA) was calculated using MINITAB 14 (Table 3). Degrees of freedom (DF), sum of squares (Seq SS), modified sum of squares (Adj SS), modified mean square (MS Adj), F statistics and P values of the model expression are listed in Table 3. Data analysis gave a semi-empirical expression of MB removal with following equation (4):

$$Y_{Predicted} \ (\%MB \ Removal) = 269.54 \ x_2 + 1.59 \ x_4 - 583.46 \ (x_2)^2 - 0.27 \ (x_3)^2 - 0.04 \ (x_4)^2 + 12.76 x_2 x_3 \qquad (4)$$

Based on the analysis of Eq. (4) depicted that the variables x_2 (adsorbent dosage) and x_4 (adsorption time) exhibited a positive relationship in the MB removal by SS/WAC/Fe$_3$O$_4$ nanocomposite.
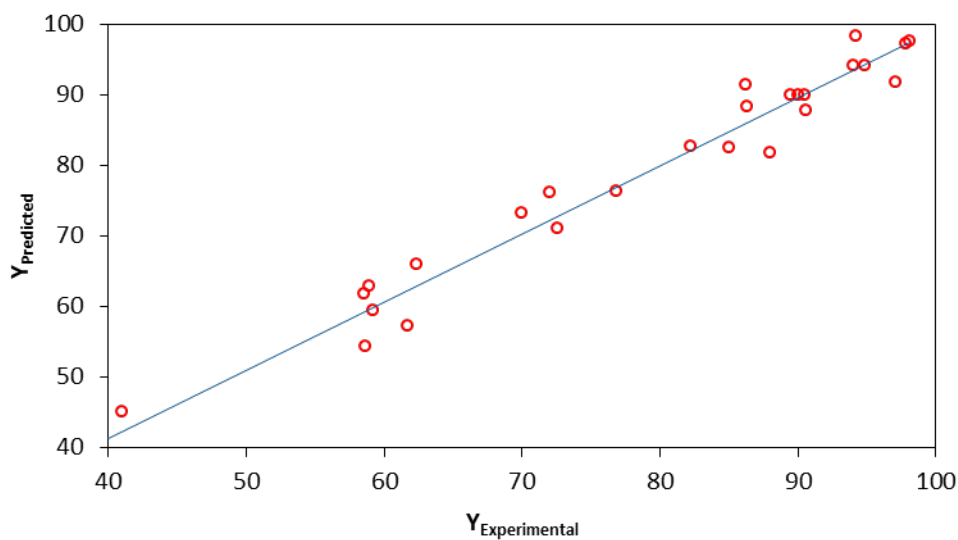

Fig. 10. The experimental data versus the predicted data of normalized removal of MB.

Table 3 Analysis of variance (ANOVA) of the response surface model for the prediction of MB removal efficiency.

Source	DF	Seq SS	Adj SS	Adj MS	F	P-Value
Regression	14	7532.04	7532.043	538.003	22.27	0.000
Linear	4	6562.49	930.043	232.511	9.62	0.001
Square	4	657.1	657.104	164.276	6.80	0.004
Interaction	6	312.45	312.452	52.075	2.16	0.121
Residual Error	12	289.91	289.911	24.159		
Lack-of-Fit	10	289.43	289.429	28.943	120.13	0.008
Pure Error	2	0.48	0.482	0.241		
Total	26	7821.95				

The results of ANOVA in Table 3 show that the F-value of the model is 120.13, which indicates that the probability that the "model F value" is high noise is only 0.01%, and most of the changes in the responses can be attributed to regression and that equations and models are meaningful [30].

The Predicted R^2 is 0.97911 was in reasonable agreement with the Adjusted R^2 (0.9200). As shown in Fig. 10, plot of experiment response ($Y_{Experimental}$) versus the predicted response indicated a good fit and it can be seen that the data points are well spaced around the straight line (R^2 = 0.9664) and confirming the statistical validation of the model [30].

The main effect plot was used to evaluate the parameters, which give high removal efficiency (Fig. 11). The main effect plot was used to evaluate para meters, which give high removal efficiency of MB (Fig. 11). Fig.11 shows sorbent dosage, in the range of 0.05-0.3 gL⁻¹. Increase the adsorbent dose to 0.25 gL⁻¹ increased the removal efficiency and the efficiency decreases become constant afterwards. Therefore, 0.25 gL⁻¹ was chosen as the optimal absorbent dosage. Addition of MB concentration upper 4.0 ppm, decreased MB

removal efficiency, as shown by the results in Fig. 11. Therefore, 4.0 ppm was chosen as the optimal MB concentration. The MB removal increased up to pH=5.5., after which that no increase was observed in MB removal efficiency until pH=7.5. Therefore, pH=6.5 was chosen as the optimal pH. This can be explained as follows: when the pH value < pH_{pzc} surface of SS/WAC/Fe$_3$O$_4$ is positively charged due to H$^+$ ion adsorption. Also methylene blue is also a cationic dye. Therefore, there is a repulsive force between the cationic dye and the adsorbent surface. In addition, at lower pH concentrations of large H$^+$ occur competitive adsorption with positively charged cationic dyes at adsorption centers. Therefore, the adsorption efficiency is low at low pH values. At pH values > pH_{pzc} surface of SS/WAC/Fe$_3$O$_4$, negatively charged by OH$^-$ adsorption and appearing electrostatic suction force between negatively charged SS/WAC/Fe$_3$O$_4$ and positive charged MB dye cause to high adsorption efficiency at large pH values [43].

Removal time which was studied in the range of 10-60 min (Fig. 11). Increasing extraction time up to 40 min increased the removal efficiency for the MB. The efficiency decreases afterwards. Thus, the optimal removal time was 40 min.
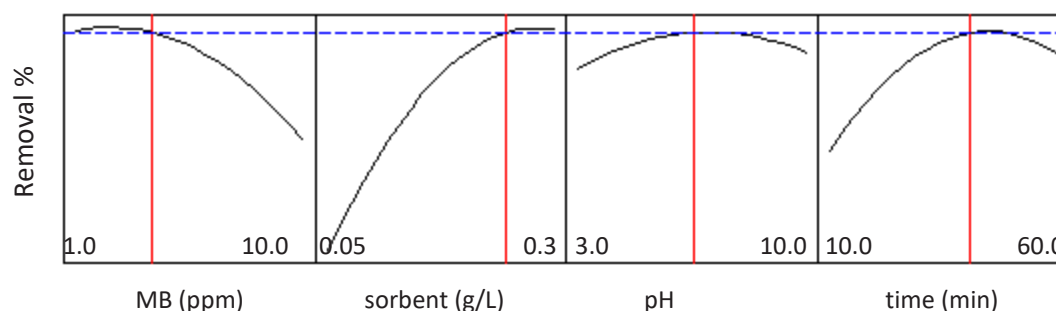

Fig. 11. The main effect plot included removal parameters and selected ranges for achieving high removal efficiency of MB.

Table 4. MB removal of different sorbents at the optimum point

sorbent	% MB Removal
SS/WAC/Fe3O4	93.61
WAC/Fe$_3$O$_4$	85.23
SS/Fe$_3$O$_4$	35.85
WAC	89.69
SS	30.33

As a result, the proposed adsorbent (0.23 g L^{-1}) is applicable for successful removal of MB (10 mg L^{-1}) in short time (40.5 min) with high adsorption capacity (37.17 mg g^{-1}). The equation of adsorption capacity is presented in Eq. 6.

Under optimal conditions, for comparison, the adsorption of methylene blue for different adsorbents was investigated and is shown in Table 4. As can be seen, the percentage of removal of MB in SS/WAC/Fe3O4 is higher than that of WAC/Fe3O4, SS/Fe3O4, WAC and SS. Certainly WAC together with the Fe$_3$O$_4$ nanoparticle properties and SS synergically improve the efficiency of adsorption procedure.

Adsorption isotherm

The adsorption isotherm provides information about the physicochemical properties of the adsorption process as a single process and are tools for describing and predicting type and intensity of the adsorbent and adsorbate interaction. In order to find a suitable model that can be utilized for design process, equilibrium data should appropriately fit into Langmuir, Freundlich and Redlich–Peterson models [44].

The accuracy of the model for predicting experimental data was evaluated with correlation coefficient (R^2) and the results are given in the table 5.

The Langmuir isotherm simulates the monolayer adsorption of the adsorbate onto homogenous adsorbent surface without migration of adsorbate molecules in the surface plane. The Langmuir isotherm equation is expressed as follows:

$$\frac{1}{q_e} = \frac{1}{ab} \cdot \frac{1}{C_e} + \frac{1}{b} \tag{5}$$
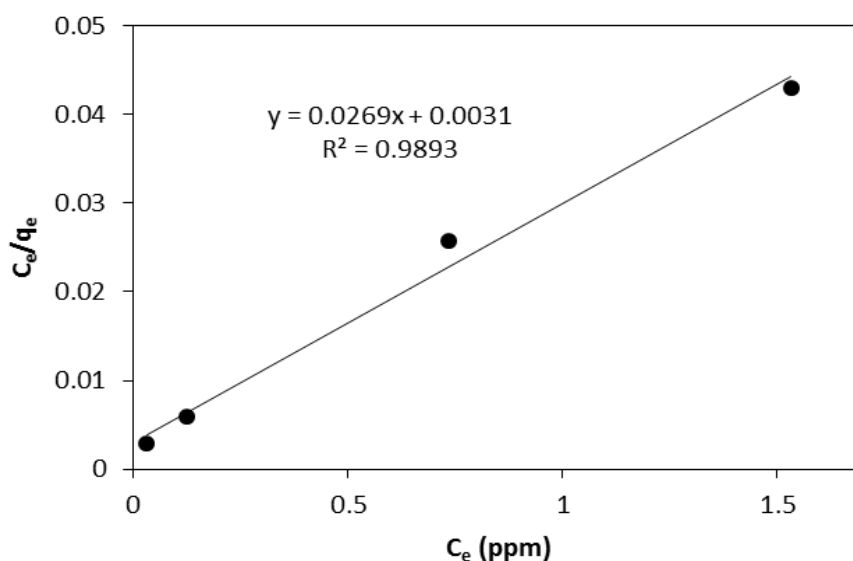

Fig. 12. Langmuir isotherm plot for adsorption of MB in adsorption conditions including pH=6.5, initial dye concentration of 1-10 mg L^{-1}, adsorbent amount of 0.232 g L^{-1} and contact time of 40 min.
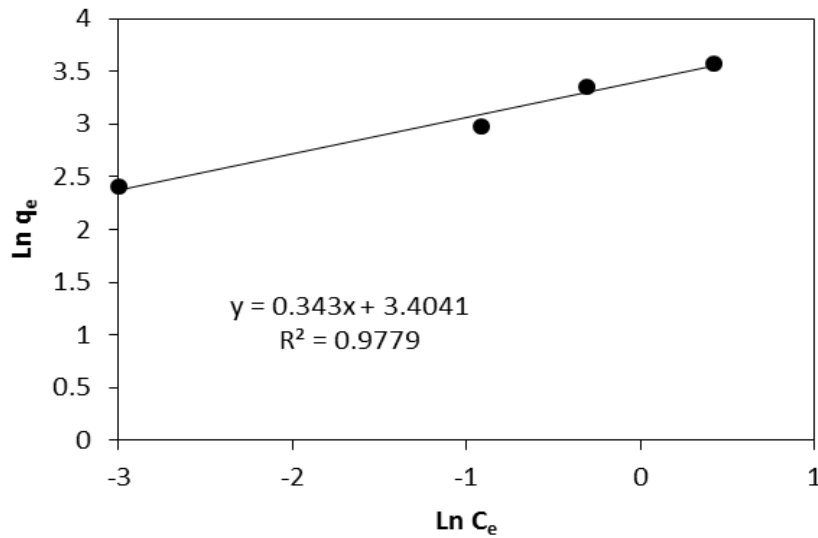
Fig. 13. Freundlich isotherm Plot for Adsorption of MB adsorption conditions including pH=6.5, initial dye concentration of 1-10 mg L^{-1}, adsorbent amount of 0.232 g L^{-1} and contact time of 40 min.

Table 5. Langmuir and Freundlich isotherm parameters for adsorption of MB by SS/WAC/Fe$_3$O$_4$ nanocomposite

Model	Equation	K	n	a(L/mg)	q$_e$(mg/g)	R^2
Langmuir	1/q$_e$=1.694(1/C$_e$)+3.771	-	-	8.67	37.17	0.9893
Freundlich	Log q$_e$=0.502Log(C$_e$)-0.371	29.2	2.9	-	-	0.9779

Where b and a are Langmuir constants related to adsorption capacity (mg/g) and adsorption equilibrium constant (l/mg), respectively. q$_e$ (adsorption capacity) is the amount of dye adsorbed at equilibrium per gram of adsorbent and it is defined as follows:

$$q_e = \frac{(c_i - c_e)}{m} \times V \qquad (6)$$

C$_i$ and C$_e$ are the initial and equilibrium concentration of dye solutions respectively (mgL^{-1}), V is the volume of the solution (l) and m is the mass (g) of the dry adsorbent used. The linear plots of 1/q$_e$ versus 1/Ce suggest the applicability of the Langmuir isotherms. The values of b and a were determined from slope and intercepts of the plots. According to the Langmuir model results (Fig. 12 and Table 5), the maximum adsorption capacity (b) and adsorption equilibrium constant (a) was 37.17 mg/g and 8.67 l/mg respectively. The larger constant values a and b indicate better absorption. The results obtained in this study, is remarkable compared to previous studies.

The Freundlich isotherm model (Fig. 13) is an exponential equation, so it is assumed that there is an interaction between adsorbed molecules on a heterogeneous surface, and it is not limited to forming a single layer. This model is given as:

$$\text{Log } q_e = 1/n \log C_e + \log K \qquad (7)$$

Where k and n are Freundlich constants related to adsorption capacity and adsorption intensity respectively. Their values are obtained from the intercept and slope respectively (Table 5) from the linear plot of logq$_e$ against logC$_e$.

The results showed that MB adsorption on the surface of SS/WAC/Fe$_3$O$_4$ nanocomposite follows the Langmuir model and has the highest correlation coefficient.

The maximum capacity (q$_e$) obtained by Langmuir isotherm for MB sorption was 37.17 mg/g for SS/WAC/Fe$_3$O$_4$ nanocomposite sorbent, which indicates the applicability of SS/WAC/Fe$_3$O$_4$ nanocomposite sorbent for treatment of real wastewater containing a high amount of understudy MB and also indicates the superiority of SS/WAC/Fe$_3$O$_4$ nanocomposite sorbent in

Table 6. Comparison of the sorption of SS/WAC/Fe$_3$O$_4$ nanocomposite by different sorbent.

Sorbent	Maximum Capacity (mg g^{-1})	Ref.
porous cellulose-derived carbon/montmorillonite	138.1	[45]
Graphene	153.8	[46]
Unburned carbon	4.2	[47]
Orange Peel	21.1	[48]
cereal chaff	20.3	[49]
garlic peel	142.8	[50]
SS/WAC/Fe$_3$O$_4$ nanocomposite	37.2	This Work

comparison to previously reported material (Table 6) and this sorbent is an effective and promising sorbent to sorption of dyes from aqueous solutions. activated carbon obtained from walnut shell contains several reaction centers, such as OH, COOH and C=O groups, which, together with the properties of nanoparticles, synergistically improve the efficiency of the adsorption process [21].

SS/WAC/Fe$_3$O$_4$ nanocomposite recyclability

The recovering and reusability test of the SS/WAC/Fe$_3$O$_4$ nanocomposite was also investigated for the removal of MB. After the completion of the reaction, the composite was separated from the MB solution by magnet and dispersed in 10 mL weak acetone solution and sonicated for 10 min and then washed with distilled water several times and then was explored for MB removal in the succeeding cycles. We repeat the above process up to five cycles. The concentration of MB in the solution is about 10 mg/L. Removal efficiency of MB was reduced from 93% in the first cycle to 85%

in final cycle (Fig. 14).

CONCLUSION

In this study, the possibility of modifying the surface of seashell with activated carbon obtained from walnut shell and Fe$_3$O$_4$ and also its efficiency to remove methylene blue dye from aqueous solution was investigated. FT-IR results showed that seashell surface modification with activated carbon and Fe$_3$O$_4$ was well done. Also, the FE-SEM image of SS/WAC/Fe$_3$O$_4$ showed that these Fe$_3$O$_4$ particles are in nanoscale and their size distribution is not wide, which increases the dye removal efficiency. In this study, effective parameters optimization was performed by optimizing the response surface methodology. Optimal adsorption conditions including pH=6.5, dye concentration of 4.0 mg L^{-1}, adsorbent amount of 0.232 g L^{-1} and contact time of 40 min were obtained. The small amount of proposed adsorbent is applicable for successful removal of MB in short time with high adsorption capacity equal to 37.2 mg g^{-1}.

The study of Langmuir and Freundlich equilibrium isotherms showed that the MB dye adsorption process on the SS/ C /Fe$_3$O$_4$ adsorbent is good and with a correlation coefficient of 0.9893 and 0.9779, respectively. The Langmuir correlation coefficient is higher than the Freundlich model, so the Langmuir isotherm is selected and introduced to predict the adsorption behavior of methylene blue dye from the aqueous medium by the adsorbent. The SS/WAC/Fe$_3$O$_4$ could be reused and recovered several times with no significant loss of adsorption capacity.

CONFLICT OF INTEREST

The authors declare that there is no conflict of interests regarding the publication of this manuscript.

REFERENCES

1. Bordbar M. Biosynthesis of Ag/almond shell nanocomposite as a cost-effective and efficient catalyst for degradation of 4-nitrophenol and organic dyes. RSC Advances. 2017;7(1):180-189.

2. Bordbar M, Mortazavimanesh N. Biosynthesis of waste pistachio shell supported silver nanoparticles for the catalytic reduction processes. IET nanobiotechnology 2018;12(7):939-945.

3. Moattari RM, Mohammadi T. Hybrid Adsorbents for Dye Removal from Wastewater. In: Inamuddin, Ahamed MI, Lichtfouse E, Asiri AM, editors. Green Adsorbents to Remove Metals, Dyes and Boron from Polluted Water. Cham: Springer International Publishing; 2021. p. 405-451.

4. McYotto F, Wei Q, Macharia DK, Huang M, Shen C, Chow CWK. Effect of dye structure on color removal efficiency by coagulation. Chem Eng J. 2021;405:126674.

5. Ben Arfi R, Karoui S, Mougin K, Ghorbal A. Adsorptive removal of cationic and anionic dyes from aqueous solution by utilizing almond shell as bioadsorbent. Euro-Mediterranean Journal for Environmental Integration. 2017;2(1):20.

6. Bordbar M, Mortazavimanesh N. Green synthesis of Pd/walnut shell nanocomposite using Equisetum arvense L. leaf extract and its application for the reduction of 4-nitrophenol and organic dyes in a very short time. Environmental Science and Pollution Research. 2017;24(4):4093-4104.

7. García JR, Sedran U, Zaini MAA, Zakaria ZA. Preparation, characterization, and dye removal study of activated carbon prepared from palm kernel shell. Environmental Science and Pollution Research. 2018;25(6):5076-5085.

8. Ramakrishna KR, Viraraghavan T. Dye removal using low cost adsorbents. Water Sci Technol. 1997;36(2-3):189-196.

9. Ho Y-S, McKay G. Sorption of dye from aqueous solution by peat. Chem Eng J. 1998;70(2):115-124.

10. Mckay G, Blair H, Gardner J. Adsorption of dyes on chitin. I. Equilibrium studies. J Appl Polym Sci. 1982;27(8):3043-3057.

11. Mc Kay G, Blair H, Gardner J. Rate studies for the adsorption of dyestuffs onto chitin. Journal of Colloid and înterface Science. 1983;95(1):108-119.

12. Juang RS, Tseng RL, Wu FC, Lee SH. Adsorption behavior of reactive dyes from aqueous solutions on chitosan. Journal of Chemical Technology & Biotechnology: International Research in Process, Environmental AND Clean Technology. 1997;70(4):391-399.

13. McKay G. Analytical solution using a pore diffusion model for a pseudoirreversible isotherm for the adsorption of basic dye on silica. AIChE journal. 1984;30(4):692-697.

14. Hu T-L. Removal of reactive dyes from aqueous solution by different bacterial genera. Water Sci Technol. 1996;34(10):89-95.

15. Namasivayam C, Prabha D, Kumutha M. Removal of direct red and acid brilliant blue by adsorption on to banana pith. Bioresour Technol. 1998;64(1):77-79.

16. Aksu Z. Biosorption of reactive dyes by dried activated sludge: equilibrium and kinetic modelling. Biochem Eng J. 2001;7(1):79-84.

17. Yang J-X, Hong G-B. Adsorption behavior of modified Glossogyne tenuifolia leaves as a potential biosorbent for the removal of dyes. J Mol Liq. 2018;252:289-295.

18. Değermenci GD, Değermenci N, Ayvaoğlu V, Durmaz E, Çakır D, Akan E. Adsorption of reactive dyes on lignocellulosic waste; characterization, equilibrium, kinetic and thermodynamic studies. Journal of Cleaner Production. 2019;225:1220-1229.

19. Roosta M, Ghaedi M, Daneshfar A, Sahraei R, Asghari A. Optimization of the ultrasonic assisted removal of methylene blue by gold nanoparticles loaded on activated carbon using experimental design methodology. Ultrason

Sonochem. 2014;21(1):242-252.

20. Ai L, Zeng C, Wang Q. One-step solvothermal synthesis of Ag-Fe₃O₄ composite as a magnetically recyclable catalyst for reduction of Rhodamine B. Catal Commun. 2011;14(1):68-73.

21. Chang C-F, Lin P-H, Höll W. Aluminum-type superparamagnetic adsorbents: synthesis and application on fluoride removal. Colloids Surf Physicochem Eng Aspects. 2006;280(1-3):194-202.

22. Banerjee SS, Chen D-H. Fast removal of copper ions by gum arabic modified magnetic nano-adsorbent. J Hazard Mater. 2007;147(3):792-799.

23. Yang N, Zhu S, Zhang D, Xu S. Synthesis and properties of magnetic Fe₃O₄-activated carbon nanocomposite particles for dye removal. Mater Lett. 2008;62(4-5):645-647.

24. Ahmad R. Studies on adsorption of crystal violet dye from aqueous solution onto coniferous pinus bark powder (CPBP). J Hazard Mater. 2009;171(1-3):767-773.

25. Oliveira LC, Rios RV, Fabris JD, Garg V, Sapag K, Lago RM. Activated carbon/iron oxide magnetic composites for the adsorption of contaminants in water. Carbon. 2002;40(12):2177-2183.

26. Pirillo S, Ferreira ML, Rueda EH. Adsorption of alizarin, eriochrome blue black R, and fluorescein using different iron oxides as adsorbents. Ind Eng Chem Res. 2007;46(24):8255-8263.

27. Bordbar M, Sharifi-Zarchi Z, Khodadadi B. Green synthesis of copper oxide nanoparticles/clinoptilolite using Rheum palmatum L. root extract: high catalytic activity for reduction of 4-nitro phenol, rhodamine B, and methylene blue. J Sol-Gel Sci Technol. 2017;81(3):724-733.

28. Razaghi Z, Aghajani Z, Faal AY. Novel synthesis and characterization of Fe₃O₄/C nanocomposits and investigation of its application in removal of pesticide diazinon. Journal of Materials Science: Materials in Electronics. 2016;27(12):13119-13126.

29. Zhang Z, Duan H, Li S, Lin Y. Assembly of magnetic nanospheres into one-dimensional nanostructured carbon hybrid materials. Langmuir. 2010;26(9):6676-6680.

30. Liu Y, Wang J, Zheng Y, Wang A. Adsorption of methylene blue by kapok fiber treated by sodium chlorite optimized with response surface methodology. Chem Eng J. 2012;184:248-255.

31. Jawad AH, Malek NNA, Abdulhameed AS, Razuan R. Synthesis of Magnetic Chitosan-Fly Ash/Fe₃O₄ Composite for Adsorption of Reactive Orange 16 Dye: Optimization by Box–Behnken Design. Journal of Polymers and the Environment. 2020;28(3):1068-1082.

32. Mazaheri H, Ghaedi M, Azqhandi MA, Asfaram A. Application of machine/statistical learning, artificial intelligence and statistical experimental design for the modeling and optimization of methylene blue and Cd (II) removal from a binary aqueous solution by natural walnut carbon. Physical Chemistry Chemical Physics. 2017;19(18):11299-11317.

33. Trinkunaite-Felsen J, Birkedal H, Zarkov A, Tautkus S, Stankeviciute Z, Kareiva A. Environmentally benign fabrication of calcium hydroxyapatite using seashells collected in Baltic Sea countries: A comparative study. Phosphorus, Sulfur Silicon Relat Elem. 2016;191(6):919-925.

34. Okoya A, Anjous-Alao R, Awokoya K. Sorption Characteristics of Halogenated Acetonitriles (HANs) in Surface Water onto Activated Carbon Prepared from Walnut Shell. International Research Journal of Pure and Applied Chemistry. 2020:273-287.

35. Shilova OA, Nikolaev AM, Kovalenko AS, Sinel'nikov AA, Kopitsa GP, Baranchikov AE. Synthesis of Magnetic Nanopowders of Iron Oxide: Magnetite and Maghemite. Russian Journal of Inorganic Chemistry. 2020;65(3):426-430.

36. Mosaddegh E, Hassankhani A. Application and characterization of eggshell as a new biodegradable and heterogeneous catalyst in green synthesis of 7, 8-dihydro-4H-chromen-5 (6H)-ones. Catal Commun. 2013;33:70-75.

37. Tang BZ, Geng Y, Sun Q, Zhang XX, Jing X. Processible nanomaterials with high conductivity and magnetizability. Preparation and properties of maghemite/polyaniline nanocomposite films. Pure and applied chemistry. 2000;72(1-2):157-162.

38. Zhang Z, Wan M. Nanostructures of polyaniline composites containing nano-magnet. Synth Met. 2003;132(2):205-212.

39. Ahmad S, Riaz U, Kaushik A, Alam J. Soft template synthesis of super paramagnetic Fe₃O₄ nanoparticles a novel technique. Journal of Inorganic and Organometallic Polymers and Materials. 2009;19(3):355-360.

40. Sahu UK, Sahu MK, Mohapatra SS, Patel RK. Removal of As (V) from aqueous solution by Ce-

Fe bimetal mixed oxide. Journal of environmental chemical engineering. 2016;4(3):2892-2899.

41. Zhang WM, Wu XL, Hu JS, Guo YG, Wan LJ. Carbon coated Fe_3O_4 nanospindles as a superior anode material for lithium-ion batteries. Adv Funct Mater. 2008;18(24):3941-3946.

42. Jung JH, Shon BH, Yoo KS, Oh KJ. Physicochemical characteristics of waste sea shells for acid gas cleaning absorbent. Korean J Chem Eng. 2000;17(5):585-592.

43. Do TH, Nguyen VT, Dung NQ, Chu MN, Van Kiet D, Ngan TTK, et al. Study on methylene blue adsorption of activated carbon made from Moringa oleifera leaf. Materials Today: Proceedings. 2021;38:3405-3413.

44. Khaled A, El Nemr A, El-Sikaily A, Abdelwahab O. Treatment of artificial textile dye effluent containing Direct Yellow 12 by orange peel carbon. Desalination. 2009;238(1-3):210-232.

45. Tong DS, Wu CW, Adebajo MO, Jin GC, Yu WH, Ji SF, et al. Adsorption of methylene blue from aqueous solution onto porous cellulose-derived carbon/montmorillonite nanocomposites. Applied Clay Science. 2018;161:256-264.

46. Liu T, Li Y, Du Q, Sun J, Jiao Y, Yang G, et al. Adsorption of methylene blue from aqueous solution by graphene. Colloids Surf B Biointerfaces. 2012;90:197-203.

47. Wang S, Li L, Wu H, Zhu ZH. Unburned carbon as a low-cost adsorbent for treatment of methylene blue-containing wastewater. Journal of Colloid and Interface Science. 2005;292(2):336-343.

48. ALzaydien AS. Adsorption of methylene blue from aqueous solution onto a low-cost natural Jordanian Tripoli. American Journal of Applied Sciences. 2009;6(6):1047.

49. Han R, Wang Y, Han P, Shi J, Yang J, Lu Y. Removal of methylene blue from aqueous solution by chaff in batch mode. J Hazard Mater. 2006;137(1):550-557.

50. Hameed BH, Ahmad AA. Batch adsorption of methylene blue from aqueous solution by garlic peel, an agricultural waste biomass. J Hazard Mater. 2009;164(2):870-875.